Chemical Doping of Large-Area Stacked Graphene Films for Use as Transparent, Conducting Electrodes

Amal Kasry,[†,‡] Marcelo A. Kuroda,[†,§] Glenn J. Martyna,[†] George S. Tulevski,[†,*] and Ageeth A. Bol[†,*]

[†]IBM T. J. Watson Research Center, 1101 Kitchawan Road, Yorktown Heights, New York 10598, [‡]Egypt Nanotechnology Research Center, Smart Village, Giza, 12577 Egypt, and [§]Department of Computer Science, University of Illinois at Urbana—Champaign, Urbana, Illinois 61801

ABSTRACT Graphene is considered a leading candidate to replace conventional transparent conducting electrodes because of its high transparency and exceptional transport properties. The effect of chemical p-type doping on graphene stacks was studied in order to reduce the sheet resistance of graphene films to values approaching those of conventional transparent conducting oxides. In this report, we show that large-area, stacked graphene films are effectively p-doped with nitric acid. The doping decreases the sheet resistance by a factor of 3, yielding films comprising eight stacked layers with a sheet resistance of 90 Ω/□ at a transmittance of 80%. The films were doped either after all of the layers were stacked (last-layer-doped) or after each layer was added (interlayer-doped). A theoretical model that accurately describes the stacked graphene film system as a resistor network was developed. The model defines a characteristic transfer length where all the channels in the graphene films actively contribute to electrical transport. The experimental data shows a linear increase in conductivity with the number of graphene layers, indicating that each layer provides an additional transport channel, in good agreement with the theoretical model.

KEYWORDS: graphene · doping · transparent conductive electrodes · solar cells · resistor network · stacking

Graphene, a single layer of graphite, possesses remarkable optical and electrical properties that have stimulated a vast amount of research in the fields of condensed matter physics and materials science.[1−4] At room temperature, charge carriers in graphene can travel thousands of interatomic distances without scattering, resulting in very high carrier mobilities.[1] In addition to the remarkable electronic properties, graphene is optically transparent and flexible and has high chemical resistance and a relatively low manufacturing cost, making graphene an ideal candidate for a transparent conducting electrode (TCE), a critical component in photovoltaic devices, displays, and touchscreens.[5−12] Although conventional TCE materials, such as indium tin oxide (ITO), have exceptional optoelectronic properties,[13] they suffer from considerable drawbacks, including increased materials costs, costs associated with vacuum deposition, and brittleness, making them unsuitable for flexible substrates.[14−16]

Several methods exist for the preparation of single- to few-layer graphene films. Solution-based methods include chemical exfoliation with organic solvents[7,17] and chemically reducing graphite oxides.[18] Graphene is also grown on metal substrates (i.e., nickel or copper) *via* chemical vapor deposition (CVD).[11,19−23] In this work, large-area graphene films were grown on Cu foils as first reported by the Ruoff group, as this growth method yields high-quality large-area films.[12,19] Despite the high-quality graphene growth, to date the sheet resistance (R_S) of a single graphene layer grown with this method (2100 Ω/□ at 97% transmittance) remains too high for the sheet to be used as a TCE.[12] Two approaches can be pursued to reduce the sheet resistance of graphene: stacking of graphene layers on top of each other and/or chemical doping. Stacking graphene layers essentially adds channels for charge transport; however, this approach simultaneously reduces the transparency of the system.[12] In addition, since the sheet resistances of the individual layers remain unchanged, alternative approaches such as chemical doping must also be considered.[7,24,25] Graphene is classified as a zero-band-gap semiconductor, where the density of states vanishes at the Dirac point. Undoped graphene has a low carrier density, and thus a high sheet resistance, as a result of its vanishing density of states at the Dirac point. Because of unintentional dopants, the Fermi level most certainly will not reside at the Dirac point of CVD-grown graphene films exposed to air, yet chemical doping further increases the carrier concentration and thus further reduces the resistance of the film.

*Address correspondence to gstulevs@us.ibm.com, ageeth@us.ibm.com.

Received for review March 11, 2010 and accepted June 25, 2010.

Published online July 12, 2010. 10.1021/nn100508g

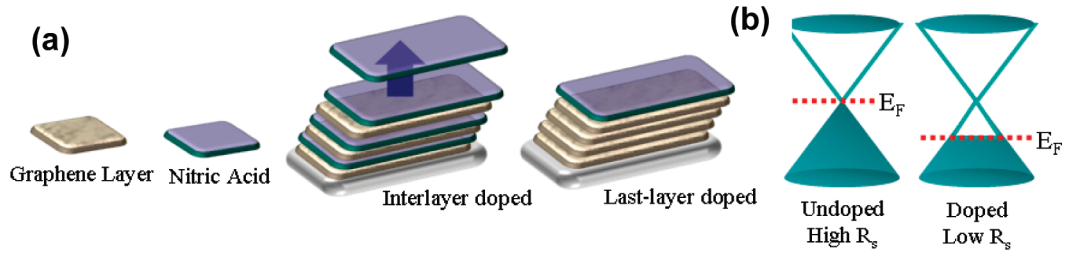

Scheme 1. (a) Schematic illustrating the two different doping methods pursued here. In the interlayer-doped case, the sample is exposed to nitric acid after each layer is stacked, whereas in the last-layer-doped case, the film is exposed to nitric acid after the final layer is stacked. (b) Illustration of the graphene band structure, showing the change in the Fermi level due to chemical p-type doping.

The key results of this report are that stacks of graphene films up to eight layers can be effectively p-doped with nitric acid. The films were doped either after each layer was stacked (interlayer-doped) or after the last layer was stacked (last-layer-doped) (see Scheme 1a). The interlayer doping method yields better optoelectronic properties. The sheet resistance is reduced by a factor of 3 upon exposure to nitric acid, yielding films with $R_S = 90\ \Omega/\square$ at a transmittance of 80% (at 550 nm). The nitric acid hole-dopes the films, increasing the carrier concentration and reducing the sheet resistance (Scheme 1b). A network resistor model was developed to describe the transport in the stacked graphene film. The model describes a characteristic channel length where all of the graphene layers are active in transport. The experimental data shows a linear increase in conductivity as a function of the number of layers, indicating that each additional layer represents an additional transport channel, in excellent agreement with the model.

RESULTS AND DISCUSSION

Figure 1a is an atomic force microscopy (AFM) image of a graphene film after it was transferred from copper to a quartz substrate. The image shows a single layer of graphene divided by several-nanometer-high folds in the film that were formed during cooling of the substrate. Once the film was transferred to a transparent substrate, a UV−vis−NIR absorption spectrum was obtained. Figure 1b shows UV−vis−NIR spectra of monolayer and trilayer graphene that were transferred individually to a quartz substrate. As expected from the band structure, the absorption spectrum is flat and rather featureless. The single layer transmits ~97% of the light at 550 nm, as expected for a single layer of graphene.[6,7] The transmittance is high over a broad spectral range, making graphene advantageous for photovoltaic applications.

Figure 2a shows plots of transmittance (measured at 550 nm) as a function of the number of graphene layers added, for both the interlayer-doped and last-layer-doped stacked graphene films (SGFs). The measured values clearly follow the Beer−Lambert law,[26] shown as the fitted black line. A higher transmittance is obtained for the interlayer-doped films than the last-layer doped films, as shown in Figure 2a. We attribute the enhanced transmission for interlayer-doped SGFs to the removal of amorphous carbon species or other impurities from each separate graphene layer by nitric acid. These impurities either can form during the graphene synthesis or are residues from the PMMA resist stripping process. In the case of last-layer-doped SGFs, the

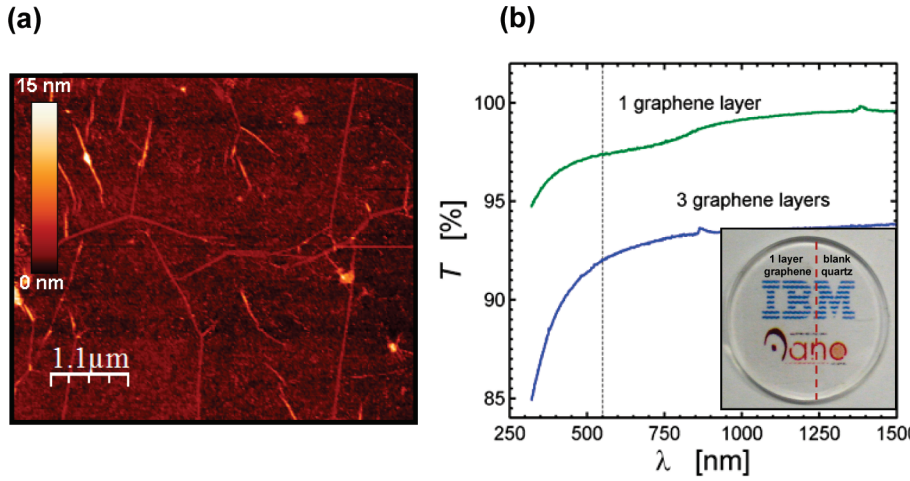

Figure 1. (a) AFM image of a single graphene layer transferred to a quartz substrate. The grains are separated by folds in the graphene generated during cooling. (b) Plots of transmittance vs wavelength for monolayer (green) and trilayer (blue) graphene on a quartz substrate. Inset: optical image of a quartz slide with half of the slide covered with a single graphene sheet.

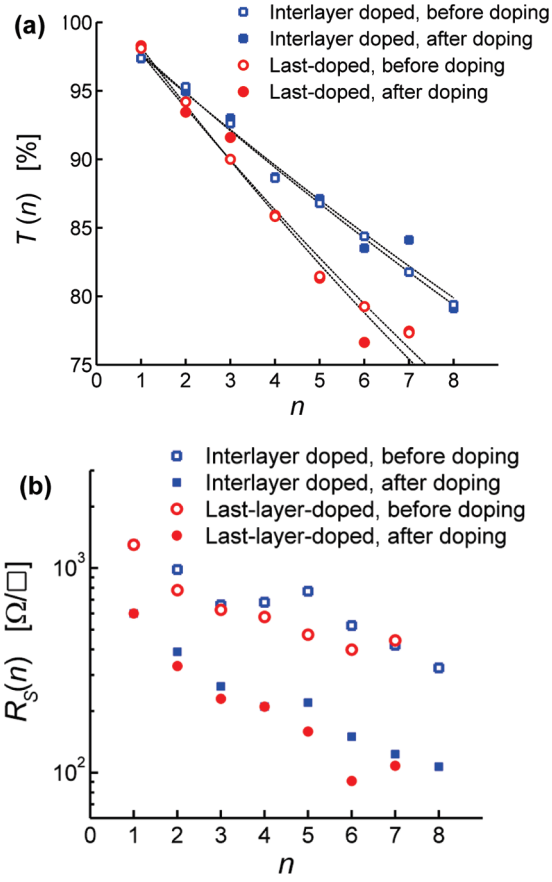

Figure 2. (a) Plots of transmittance {T(*n*) [%] at 550 nm} as a function of the number of graphene layers *n* for both the interlayer-doped (blue data) and the last-layer-doped (red data) cases. The black lines are fits using the Beer−Lambert law. Interlayer doping produces films with higher transmittance values. (b) Plots of the sheet resistance (R_S) as a function of the number of graphene layers for both the interlayer-doped (blue) and last-layer-doped (red) cases before and after doping. The sheet resistance is reduced by a factor of 3 with nitric acid doping.

graphene system is exposed to nitric acid after the stacking is complete, leaving possible impurities between the layers, which lowers the total transmittance of the stack. In the interlayer-doped case, the transmittance decreases by ~2.5% for each added layer, indicating that the film behaves as a set of individual graphene layers.[6,7]

HNO_3 is known to be a p-type dopant in graphitic materials (i.e., graphite and carbon nanotubes),[27−30] where an electron is transferred from the graphene to the nitric acid as a charge-transfer complex is formed according to the reaction[30]

$$6HNO_3 + 25C \rightarrow C_{25}^{+}NO_3^{-}\cdot 4HNO_3 + NO_2 + H_2O$$

This results in a shift of the Fermi level, which increases the carrier concentration and thus the conductivity of the graphene layers, as shown in Scheme 1b. This effect was observed with single-walled carbon nanotubes (SWCNTs), where the doping of the SWCNTs with nitric acid led to an increase in the conductivity of SWCNT

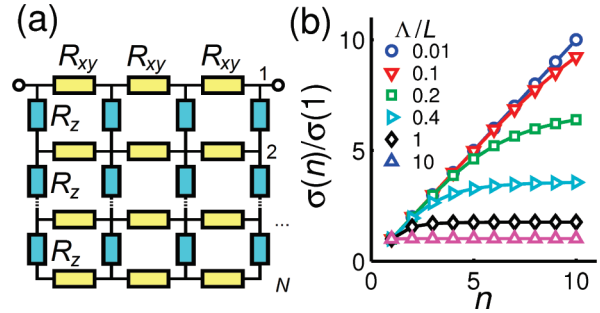

Figure 3. (a) Illustration of the resistor network model describing the stacked graphene films. (b) Effective sheet conductance σ in a four-point probe configuration as a function of the number of graphene layers *n* for values of the ratio Λ/*L* = 0.01, 0.1, 0.2, 0.4, 1, and 10. As *L* increases, more channels are active in transport, as indicated by an absence of saturation in the curve.

films.[27−29] Since SWCNTs and graphene have essentially the same chemical structure, it is not surprising that HNO_3 would also dope graphene, yielding films with a lower sheet resistance. Additionally, HNO_3 intercalates of graphite were extensively studied and shown to increase in conductivity.[31] Previous work showed a higher in-plane conductivity for intercalated graphite ($1.6 \times 10^5\ \Omega^{-1}\ cm^{-1}$) than for pristine graphite ($2.5 \times 10^4\ \Omega^{-1}\ cm^{-1}$) at room temperature.[31]

The sheet resistance as a function of the number of graphene layers for both the interlayer-doped and last-layer-doped films is shown in Figure 2b. In both cases, R_S is reduced by a factor of 3, indicating efficient p-type doping with nitric acid. The resistance was comparable in the interlayer-doped and last-layer-doped cases, which is due to one of two possibilities: first, nitric acid could intercalate into the graphene stacks, resulting in equivalently doped films; second, since nitric acid is volatile, the dopant could evaporate before another layer is added, yielding equivalently doped films. Since the sheet resistances of the two films are similar and the optical data (Figure 2a) show that interlayer doping yields a higher transmittance, only the interlayer doping method will be considered for the remainder of this report.

As shown in Figure 2b, R_S in both cases is proportional to 1/*n*, where *n* is number of stacked graphene layers. This observation agrees well with a theoretical model describing the current flow in an SGF as a resistor network, as depicted in Figure 3a. According to this model, the in-plane current density at the *i*th layer ($\mathbf{j}_i$) is given by the following formula (see the Supporting Information):

$$\frac{R_S}{\rho}[\mathbf{j}_{i+1}(\mathbf{r}) - \mathbf{j}_i(\mathbf{r})] = -\sum_{i'=1}^{i} \nabla(\nabla\cdot\mathbf{j}_{i'})$$

where R_S and ρ are the in-plane sheet resistance and interlayer resistivity, respectively. In the previous equation, a characteristic length Λ can be defined as follows:

$$\Lambda = \sqrt{\frac{\rho}{R_S}}$$

This length represents the distance that the current, if not injected evenly into the two graphene films, should flow before becoming homogeneously distributed across them. This length can be layer-dependent if either the in-plane or the out-of-plane conductivity varies across different films as a result of, for example, the presence of an external gate or nonuniform doping. In our case, we have assumed that both the in-plane sheet resistance and the out-of-plane conductivity are constant and considered a four-point probe system[32] in which the probes are separated by a distance L and all of the current is injected into the top film. Figure 3b shows the effective sheet conductance of an SGF obtained using the resistor network model as a function of the number of layers, normalized by the sheet conductance of a single film. We have neglected the fact that the in-plane resistivity in monolayer graphene has been reported to be larger than that in bilayer graphene because the effects of charged impurities in the substrate are screened by the first layer.[33] For $L \ll \Lambda$, the system exhibits the same sheet conductance regardless of the number of stacked layers because of the poor interlayer conductivity (*i.e.*, all of the current flows in the top layer). On the other hand, when $L \gg \Lambda$, increasing the number of films adds channels in parallel, resulting in a conductance decrease that is inversely proportional to the number of films. When $L \approx \Lambda$, the sheet conductance saturates after a certain number of layers. In SGF systems, the magnitude of Λ can be estimated in terms of the in-plane and out-of-plane conductivities (σ_{xy} and σ_z, respectively) and the interlayer separation of graphite ($a_0 = 0.34$ nm)[31] as:

$$\Lambda \approx \sqrt{\frac{\sigma_{xy}}{\sigma_z}} a_0 \approx 100 \text{ nm}$$

Therefore, the current density in an SGF system may not be homogeneous across the different films in nanoscale devices.[34] However, for typical four-point probe measurements, where the distance between electrodes is on the order of millimeters ($L \gg \Lambda$), all of the films can be assumed to carry the same amount of current. Since R_S is directly proportional to $1/n$, it becomes convenient to characterize experimentally the effective sheet conductance rather than the sheet resistance, since the former magnitude in macroscopic SGF systems scales linearly with the number of layers, as depicted in Figure 4. Figure 4 shows that the fitted data based on this model are in very good agreement with the experimental results for both undoped and doped SGF systems. As clearly shown in Figure 4, there is a significant decrease in the sheet resistance after the HNO_3 doping. The sheet conductance increases linearly with the number of layers, indicating that each additional layer is an active channel for transport.

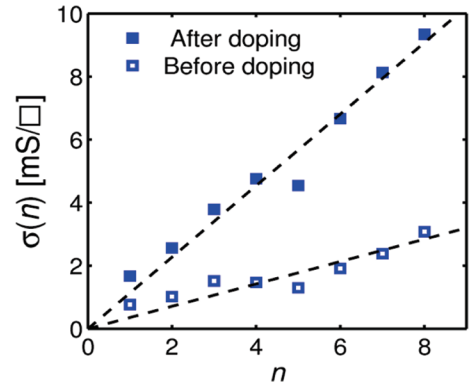

Figure 4. Fitting of the sheet conductance σ as a function of the number of graphene layers *n* using the resistor network model for the interlayer-doped system before and after doping. The fitted data are in very good agreement with the experimental values. The dotted lines represent the model, while the blue squares represent the experimental results. The sheet conductance increases linearly with the number of graphene layers, indicating that each additional layer is an active channel for transport.

Figure 5 shows plots of transmittance versus sheet resistance for SGFs in which the films were interlayer-doped. Each point represents the addition of a graphene layer before (○) or after (●) doping. The resistance decreases with transparency as additional transport channels are added. The sheet resistance decreases by a factor of 3 upon doping with nitric acid, reaching a minimum value of 90 Ω/□ at a transmittance of 80%. This result highlights the potential of graphene as a TCE, since films with a transmittance of 93% have a resistance of ~250 Ω/□, a value already suitable for many display applications.

CONCLUSION

In conclusion, we have studied the electrical and optical properties of large-area stacked graphene films (up to eight layers) that were effectively p-doped with nitric acid. The p-doping reduces the sheet resistance

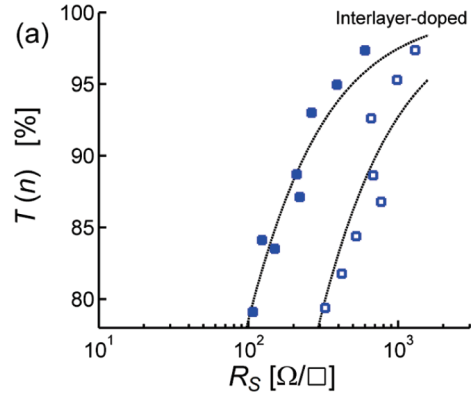

Figure 5. (a) Plot of transmittance {*T*(*n*) [%] at 550 nm} vs sheet resistance R_S before (○) and after (●) doping with nitric acid. The curves are guidelines for visual purposes only.

by a factor of 3. Films formed by interlayer doping exhibited higher performance than films formed by last-layer doping because of their higher transmittance. A resistor network model that describes a characteristic length above which all the layers contribute to transport was developed. The experimental results show that in agreement with the theoretical model, the conductance of large-area graphene films increases linearly with the number of layers but its optical transmittance decreases by ~2.5% per graphene sheet. A sheet resistance of 90 Ω/□ at a transmittance of 80% was achieved. The measured sheet resistance approaches values of conventional TCEs and is already suitable for some applications, especially where high transmittance is required. The lack of a percolation threshold and the exceptional mechanical and electrical properties highlight the potential of graphene films for applications where high transmittance values are required.

EXPERIMENTAL METHODS

A piece of Cu foil (25 μm thick, Sigma-Aldrich) was placed in a 1 in. diameter quartz furnace tube at low pressure (60 mTorr). Prior to processing, the system was flushed with 6 sccm of forming gas (5% H_2 in Ar) for 2 h at a pressure of ~500 mTorr to remove any residual oxygen and water present in the system. The concentrations of oxygen and water in the chamber were monitored with a residual gas analyzer (Ametek, Dycor Dymaxion). The Cu foil was then heated to 875 °C in forming gas (6 sccm, 500 mTorr) and kept at this temperature for 30 min to reduce native CuO and increase the Cu grain size. After reduction, the Cu foil was exposed to ethylene (6 sccm, 500 mTorr) at 875 °C for 30 min. The sample was cooled in forming gas (6 sccm, 500 mTorr). PMMA was spin-coated on top of the graphene layer formed on the Cu foil, and the Cu foil was then dissolved in 1 M iron (III) chloride. The remaining graphene/PMMA layer was thoroughly washed with deionized water and transferred to a quartz substrate. Subsequently, the PMMA was dissolved in hot acetone (80 °C) for 1 h. The substrate with graphene was rinsed in methanol and dried in a stream of nitrogen. Multilayers of graphene were prepared by stacking individually grown graphene layers on top of each other until the desired number of layers was obtained. After each graphene layer addition, a transmission spectrum (Perkin-Elmer Lambda 950 UV−vis spectrometer) was obtained using a blank quartz sample as a reference for subtraction. The sheet resistance was also measured using a manual four-point probe apparatus (Signatone, probe distance 1.5 mm). The sheet resistance was calculated using the following equation:

$$R_S = \frac{\pi}{\ln 2}\frac{V}{I} = 4.5324\frac{V}{I}$$

Two different doping schemes were pursued, as shown schematically in Scheme 1a. In the first scenario (interlayer doping), every graphene layer was doped with nitric acid (HNO_3) as it was added to the stack. In the second scenario (last-layer doping), the doping was done at the end of the stacking process. Doping with nitric acid was achieved by placing the graphene layers on quartz in concentrated HNO_3 (65%) for 5 min followed by drying with a stream of nitrogen. In both scenarios, the transmission and sheet resistance were measured before and after each step of stacking and doping. In the text and in the graphs, "before doping" and "after doping" mean before and after exposure of the films to HNO_3, respectively, for both interlayer-doped and last-layer-doped systems.

Acknowledgment. This work was conducted under and partially funded by the 2008 joint development agreement between IBM Research and the Government of the Arab Republic of Egypt through the Egypt Nanotechnology Center (EGNC; http://www.egnc-ibm.gov.eg/).

Supporting Information Available: Description of the network resistor model. This material is available free of charge *via* the Internet at http://pubs.acs.org.

REFERENCES AND NOTES

1. Geim, A. K.; Novoselov, K. S. The Rise of Graphene. *Nat. Mater.* **2007**, *6*, 183–191.
2. Geim, A. K. Graphene: Status and Prospects. *Science* **2009**, *324*, 1530–1534.
3. Zhang, Y.; Tan, J. W.; Stormer, H. L.; Kim, P. Experimental Observation of the Quantum Hall Effect and Berry's Phase in Graphene. *Nature* **2005**, *438*, 201–204.
4. Novoselov, K. S.; Geim, A. K.; Morozov, S. V.; Jiang, D.; Zhang, Y.; Dubonos, S. V.; Grigorieva, I. V.; Firsov, A. A. Electric Field Effect in Atomically Thin Carbon Films. *Science* **2004**, *306*, 666–669.
5. Watcharotone, S.; Dikin, D. A.; Stankovich, S.; Piner, R.; Jung, I.; Dommett, G. H. B.; Evmenenko, G.; Wu, S. E.; Chen, S. F.; Liu, C. P.; Nguyen, S. T.; Ruoff, R. S. Graphene−Silica Composite Thin Films as Transparent Conductors. *Nano Lett.* **2007**, *7*, 1888–1892.
6. Nair, R. R.; Blake, P.; Grigorenko, A. N.; Novoselov, K. S.; Booth, T. J.; Stauber, T.; Peres, N. M. R.; Geim, A. K. Fine Structure Constant Defines Visual Transparency of Graphene. *Science* **2008**, *320*, 1308.
7. Blake, P.; Brimicombe, P. D.; Nair, R. R.; Booth, T. J.; Jiang, D.; Schedin, F.; Ponomarenko, L. A.; Morozov, S. V.; Gleeson, H. F.; Hill, E. W.; Geim, A. K.; Novoselov, K. S. Graphene-Based Liquid Crystal Device. *Nano Lett.* **2008**, *8*, 1704–1708.
8. Wang, X.; Zhi, L.; Müllen, K. Transparent, Conductive Graphene Electrodes for Dye-Sensitized Solar Cells. *Nano Lett.* **2008**, *8*, 323–327.
9. Li, X.; Zhang, G.; Bai, X.; Sun, X.; Wang, X.; Wang, E.; Dai, H. Highly Conducting Graphene Sheets and Langmuir−Blodgett Films. *Nat. Nanotechnol.* **2008**, *3*, 538–542.
10. Becerril, H. A.; Mao, J.; Liu, Z.; Stoltenberg, R. M.; Bao, Z.; Chen, Y. Evaluation of Solution-Processed Reduced Graphene Oxide Films as Transparent Conductors. *ACS Nano* **2008**, *2*, 463–470.
11. Kim, K. S.; Zhao, Y.; Jang, H.; Lee, S. Y.; Kim, J. M.; Kim, K. S.; Ahn, J.-H.; Kim, P.; Choi, J.-Y.; Hong, B. H. Large-Scale Pattern Growth of Graphene Films for Stretchable Transparent Electrodes. *Nature* **2009**, *457*, 706–710.
12. Li, X.; Zhu, Y.; Cai, W.; Borysiak, M.; Han, B.; Chen, D.; Piner, R. D.; Colombo, L.; Ruoff, R. Transfer of Large-Area Graphene Films for High-Performance Transparent Conductive Electrodes. *Nano Lett.* **2009**, *9*, 4359–4363.
13. Choi, K. H.; Kim, J. Y.; Lee, Y. S.; Kim, H. J. ITO/Ag/ITO Multilayer Films for the Application of a Very Low Resistance Transparent Electrode. *Thin Solid Films* **1999**, *341*, 152–155.
14. Chen, Z.; Cotterell, B.; Wang, W.; Guenther, E.; Chua, S. J. A Mechanical Assessment of Flexible Optoelectronic Devices. *Thin Solid Films* **2001**, *394*, 201–205.
15. Leterrier, Y.; Médico, L.; Demarco, F.; Månson, J.-A. E.; Betz, U.; Escolà, M. F.; Kharrazi, M.; Atamny, F. Mechanical Integrity of Transparent Conductive Oxide Films for Flexible Polymer-Based Displays. *Thin Solid Films* **2004**, *460*, 156–166.
16. Hass, J.; de Heer, W. A.; Conrad, E. H. The Growth and Morphology of Epitaxial Multilayer Graphene. *J. Phys.: Condens. Matter* **2008**, *20*, 323202.
17. Hernandez, Y.; Nicolosi, V.; Lotya, M.; Blighe, F. M.; Sun, Z.; De, S.; McGovern, I. T.; Holland, B.; Byrne, M.; Gun'Ko, Y. K.;

Boland, J. J.; Niraj, P.; Duesberg, G.; Krishnamurthy, S.; Goodhue, R.; Hutchison, J.; Scardaci, V.; Ferrari, A. C.; Coleman, J. N. High-Yield Production of Graphene by Liquid-Phase Exfoliation of Graphite. *Nat. Nanotechnol.* **2008**, *3*, 563–568.
18. Park, S.; Ruoff, R. S. Chemical Methods for the Production of Graphenes. *Nat. Nanotechnol* **2009**, *4*, 217–224.
19. Li, X. S.; Cai, W. W.; An, J. H.; Kim, S.; Nah, J.; Yang, D. X.; Piner, R. D.; Velamakanni, A.; Jung, I.; Tutuc, E.; Banerjee, S. K.; Colombo, L.; Ruoff, R. S. Large-Area Synthesis of High-Quality and Uniform Graphene Films on Copper Foils. *Science* **2009**, *324*, 1312–1314.
20. Sutter, P. W.; Flege, J.-I.; Sutter, E. A. Epitaxial Graphene on Ruthenium. *Nat. Mater.* **2008**, *7*, 406–411.
21. Coraux, J.; N'Diaye, A. T.; Busse, C.; Michely, T. Structural Coherency of Graphene on Ir(111). *Nano Lett.* **2008**, *8*, 565–570.
22. Yu, Q.; Lian, J.; Siriponglert, S.; Li, H.; Chen, Y. P.; Pei, S.-S. Graphene Segregated on Nickel Surfaces and Transferred to Insulators. *Appl. Phys. Lett.* **2008**, *93*, 113103.
23. Reina, A.; Jia, X.; Ho, J.; Nezich, D.; Son, H.; Bulovic, V.; Dresselhaus, M. S.; Kong, J. Large Area, Few-Layer Graphene Films on Arbitrary Substrates by Chemical Vapor Deposition. *Nano Lett.* **2009**, *9*, 30–35.
24. Jung, N.; Kim, N.; Jockusch, S.; Turro, N. J.; Kim, P.; Brus, L. Charge Transfer Chemical Doping of Few Layer Graphenes: Charge Distribution and Band Gap Formation. *Nano Lett.* **2009**, *9*, 4133–4137.
25. Farmer, B.; Golizadeh-Mojarad, R.; Perebeinos, V.; Lin, Y. M.; Tulevski, G. S.; Tsang, J. C.; Avouris, P. Chemical Doping and Electron−Hole Conduction Asymmetry in Graphene Devices. *Nano Lett.* **2009**, *9*, 388–392.
26. Skoog, D. A.; West, D. M.; Holler, F. J. *Transparencies To Accompany Fundamentals of Analytical Chemistry*; Saunders College Publishing: Philadelphia, 1988.
27. Zhou, W.; Vavro, J.; Nemes, N. M.; Fischer, J. E.; Borondics, F.; Kamarás, K.; Tanner, D. B. Charge Transfer and Fermi Level Shift in p-Doped Single-Walled Carbon Nanotubes. *Phys. Rev. B* **2005**, *71*, 205423.
28. Parekh, B. B.; Fanchini, G.; Eda, G.; Chhowalla, M. Improved Conductivity of Transparent Single-Wall Carbon Nanotube Thin Films *via* Stable Postdeposition Functionalization. *Appl. Phys. Lett.* **2007**, *90*, 121913.
29. Barnes, T. M.; Blackburn, J. L.; van de Lagemaat, J.; Coutts, T. J.; Heben, M. J. Reversibility, Dopant Desorption, and Tunneling in the Temperature-Dependent Conductivity of Type-Separated, Conductive Carbon Nanotube Networks. *ACS Nano* **2008**, *2*, 1968–1976.
30. Fillaux, F.; Menu, S.; Conard, J.; Fuzellier, H.; Parker, S. W.; Hanon, A. C.; Tomkinson, J. Inelastic Neutron Scattering Study of the Proton Dynamics in HNO_3 Graphite Intercalation Compounds. *Chem. Phys.* **1999**, *242*, 273–281.
31. Dresselhaus, M. S.; Dresselhaus, G. Intercalation Compounds of Graphite. *Adv. Phys.* **2002**, *51*, 1–186.
32. Smits, F. M. Measurement of Sheet Resistivities with the Four Point Probe. *Bell Syst. Tech. J.* **1958**, *37*, 711–718.
33. Lin, Y. M.; Avouris, P. Strong Suppression of Electrical Noise in Bilayer Graphene Nanodevices. *Nano Lett.* **2008**, *8*, 2119–2125.
34. Sui, Y.; Appenzeller, J. Screening and Interlayer Coupling in Multilayer Graphene Field-Effect Transistors. *Nano Lett.* **2009**, *9*, 2973–2977.